JACS
JOURNAL OF THE AMERICAN CHEMICAL SOCIETY

Article

pubs.acs.org/JACS

Re-entrant Lithium Local Environments and Defect Driven Electrochemistry of Li- and Mn-Rich Li-Ion Battery Cathodes

Fulya Dogan,[†,∥] Brandon R. Long,[†,∥] Jason R. Croy,[†] Kevin G. Gallagher,[†] Hakim Iddir,[‡] John T. Russell,[‡] Mahalingam Balasubramanian,*[,§] and Baris Key*[,†]

[†]Chemical Sciences and Engineering Division, [‡]Materials Sciences Division, and [§]X-ray Science Division, Advanced Photon Source, Argonne National Laboratory, Argonne, Illinois 60439, United States

Supporting Information

ABSTRACT: Direct observations of structure−electrochemical activity relationships continue to be a key challenge in secondary battery research. ^{6}Li magic angle spinning (MAS) nuclear magnetic resonance (NMR) spectroscopy is the only structural probe currently available that can *quantitatively* characterize local lithium environments on the subnanometer scale that dominates the free energy for site occupation in lithium-ion (Li-ion) intercalation materials. In the present study, we use this local probe to gain new insights into the complex electrochemical behavior of activated $0.5^6Li_2MnO_3 \cdot 0.5^6LiMn_{0.5}Ni_{0.5}O_2$, lithium- and manganese-rich transition-metal (TM) oxide intercalation electrodes. We show direct evidence of path-dependent lithium site occupation, correlated to structural reorganization of the metal oxide and the electrochemical hysteresis, during lithium insertion and extraction. We report new ^{6}Li resonances centered at ∼1600 ppm that are assigned to $LiMn_6$-TM_{tet} sites, specifically, a hyperfine shift related to a small fraction of re-entrant tetrahedral TMs (Mn_{tet}), located above or below lithium layers, coordinated to $LiMn_6$ units. The intensity of the TM layer lithium sites correlated with tetrahedral TMs loses intensity after cycling, indicating limited reversibility of TM migrations upon cycling. These findings reveal that defect sites, even in dilute concentrations, can have a profound effect on the overall electrochemical behavior.

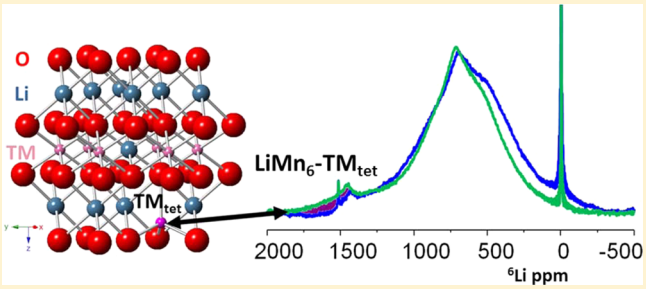

INTRODUCTION

Researchers worldwide are searching for new electrochemical energy storage materials that meet the stringent energy density, life, cost, and safety requirements of batteries for electric vehicle (EV) applications.[1,2] Layered lithium- and manganese-rich, transition-metal (TM) oxide (LMR-NMC, where TM is Ni, Mn, and Co) intercalation cathode structures have been widely investigated since 2000 as the next generation cathodes for advanced lithium-ion (Li-ion) batteries.[3−5] The promise of LMR-NMC composite electrode structures is that, when paired with an appropriate advanced anode, the resulting battery pack meets the United States Advanced Battery Consortium's EV battery system goals of <$125/kWh with energy densities over 500Wh/L.[3] These transformational cost and performance values are enabled by Li- and Mn-rich compositions that increase specific energy and energy density through high specific capacity (>230 mAh/g). This class of materials, denoted as $xLi_2MnO_3 \cdot (1-x)LiMO_2$ (M = Mn, Ni, Co), possesses complex nanocomposite structures consisting of two distinctly different, average local environments;[6,7] one rich in Li and Mn (e.g., Li_2MnO_3) and the other in the constituent TMs (e.g., $LiMO_2$). In order to achieve reversible capacities >200 mAh/g, electrochemical activation of the Li- and Mn-rich component above ∼4.4 V is necessary. However, activation followed by cycling above ∼4.0 V results in continuous structural changes to the material. Hysteresis in the open-circuit voltage is one manifestation associated with high-voltage cycling after the activation process.[8] In addition, a continuous decrease in the average voltage (energy) of cells, known as voltage fade, also occurs.[9−11] Hysteresis and voltage fade are correlated and can be quantified electrochemically.[9,10] Furthermore, both phenomena scale in magnitude with the amount of Li and Mn ordering (e.g, Li_2MnO_3 content) that is present in as-prepared compositions.[6]

The electrochemical redox process associated with the high capacities of LMR-NMC electrodes, in some examples[12] over 300 mAh/g, is still lacking a definitive explanation. However, the available literature clearly demonstrates that redox processes are correlated with structural phenomena between charge and discharge that are mostly reversible, but inherently lead to significant structural[5,13−17] rearrangements. Gallagher et al. proposed a structural model relating hysteresis and voltage fade that includes partially reversible migration of TMs and/or Li, driven by the presence of vacancies in the lithium layers.[10] The hypothesized model is founded on experimental observations of LMR-NMC electrodes as well as the currently accepted historical understanding of structural transformations

Received: November 8, 2014
Published: January 29, 2015

DOI: 10.1021/ja511299y
J. Am. Chem. Soc. 2015, 137, 2328−2335

in layered oxide intercalation hosts.[18,19] TM migration has been experimentally observed for several other layered and composite intercalation compounds such as $LiMnO_2$,[20] $LiVO_2$,[21] $Li_{1.2}Mn_{0.4}Cr_{0.4}O_2$,[22] and $LiMn_{0.5}Ni_{0.5}O_2$.[23] The migration of TMs into lithium layers is predicted by computation to involve tetrahedral sites of the lithium layers, creating "dumbbells" involving Li and, e.g., Mn.[14,23−25] This defect in the oxide structure forms across an octahedral vacancy (□) in the TM layer creating Li_{Tet}-□-Mn_{Tet} and Li_{Tet}-□-Li_{Tet} configurations. Dumbbell formation should have a direct impact on Li site energies and likely results in an observable change in lithium local environments, depending on the concentration of dumbbells formed. Likewise, the path-dependent nature of lithium site occupation may be characterized by local probes in a material that undergoes reversible (e.g., hysteresis) and irreversible (e.g., voltage fade) transformations. Of the possible local structure techniques, X-ray absorption spectroscopy, due to its averaging nature, is not very effective in elucidating the structure of potential dilute TM probe atoms in defect sites when the same element is present in both defect and regular lattice sites. The XAFS signal is dominated by the contribution of the majority probe atoms occupying regular sites, thereby rendering less sensitivity to the structure of the minority defect site. Diffraction methods are not effective either, as they require the defect to be ordered over the long-range and further lack sensitivity to low defect concentrations. More specifically in the case of neutron diffraction refinements, as already pointed by Armstrong et al. in the case of the $LiMnO_2$ system, the contribution of Li and Mn cannot be distinguished when they occupy defect sites.[20] The situation is only further exasperated in Ni containing samples as Ni could potentially also occupy the defect sites.

NMR spectroscopy has been effectively used in the past to reveal the local structures associated with lithium and TMs in battery materials.[14,24,26−38] A limitation of these earlier studies that prevented a fully quantitative, local structural analysis was the dilution of ^{6}Li environments upon cycling and the associated signal-to-noise issues. To overcome these issues, in addition to the use of ^{6}Li-enriched metal oxides, it is essential to use fully enriched cell components (electrolytes and ^{6}Li-anode) to achieve the high resolution required to study specific local structures of interest. We have undertaken an isotopic enrichment strategy coupled with very long acquisition times to obtain unprecedented, and quantitative, high-resolution data for cycled electrodes using fully enriched cell components. This strategy has allowed the determination of structure−activity relationships not yet reported. Herein, ^{6}Li MAS NMR spectroscopy is to monitor the evolution of local order and low concentration defect formation with the goal of correlating local structural changes with hysteresis and voltage fade phenomena.

EXPERIMENTAL SECTION

$(MnNi)C_2O_4$ precursors were prepared from $MnSO_4{\cdot}H_2O$, $NiSO_4{\cdot}7H_2O$, and $Na_2C_2O_4$. An aqueous solution containing the required stoichiometric amounts of metal sulfates was added under stirring into a solution of sodium oxalate. The solution was then stirred for 3 h at 70 °C. The coprecipitated powder was filtered, washed, and dried in air at 105 °C. A portion of the dried powder was thoroughly mixed with stoichiometric amounts of fully enriched ^{6}Li carbonate (Cambridge Isotopes) and annealed at 550 °C for 12 h in air, followed by grinding and annealing at 850 °C for 12 h (also in air) to prepare materials with a desired composition, 0.5 $^6Li_2MnO_3{\cdot}0.5$ $^6LiMn_{0.5}Ni_{0.5}O_2$.

Cathodes for the electrochemical tests were prepared by coating Al foil with a slurry containing 82 wt % of the oxide powder, 8 wt % super P carbon, and 10 wt % polyvinylidene difluoride (PVDF) binder in NMP and assembled in coin cells (size 2032). Typical active material loadings were 11 mg/cm^2. The cells contained an enriched ^{6}Li metal anode which was cut and then rinsed with hexanes to remove oil before use. The electrolyte was a 1 M solution of fully enriched $^6LiPF_6$ (Aldrich) in a 1:1 mixture of ethylene carbonate (EC) and dimethyl carbonate (DMC). Coin cells were assembled in a glovebox under an inert argon atmosphere. Cycling tests were performed in a temperature-controlled oven at 30 °C. All cells were subjected to a first cycle activation between 4.7−2.0 V at 5 mA/g. Cell to cell first discharge electrochemical reproducibility was ensured within ±1%. The second cycle electrochemistry, as detailed in the text, was also performed at 5 mA/g. After electrochemical testing the cells were immediately disassembled in an Ar-filled glovebox with an oxygen and water content both below 0.5 ppm. The cathodes were rinsed with anhydrous DMC to remove electrolyte and dried in Ar before NMR characterization.

^{6}Li MAS NMR experiments were performed at 7.02 T (300 MHz) on a Bruker Avance III HD spectrometer operating at a Larmor frequency of 44.21 MHz, using a 1.3 mm MAS probe. All spectra were acquired at 67 kHz with a rotor synchronized echo pulse sequence (90°-τ-180°-τ-acq), where $\tau = 1/\nu_r$. A $\pi/2$ pulse width of 1.5 μs was used with sufficiently long pulse recycle delays of 0.2 s. All spectra were collected immediately after drying (1−2 h) with 1,024,000 scans at a constant temperature of 283 ± 0.1 K (crucial for accurate and consistent determination of NMR shift trends, see Supporting Information, p S3). Chemical shifts were referenced to 1 M LiCl at 0 ppm. The spectra were normalized by the total number of scans which was the same for all runs and the weight of active materials packed in the rotors for the best possible quantitative analyses of intensity changes of each lithium resonance. Under the experimental conditions mentioned above (1 rotor period echo pulse at 67 kHz), the effect of T_2 relaxation variations has no effect on relative intensity of lithium peaks (see Figure S5 for detailed analysis). No line broadening function and identical phasing values were used for the data processing.

RESULTS AND DISCUSSION

Path-Dependent Lithium Site Occupancy and Electrochemical Hysteresis. Tracking changes in local lithium environments is required to gain insights into the electrochemical potential of lithium as a function of path-dependent site occupation. Therefore, we first performed a detailed study of lithium extraction and insertion, after activation, through a quantitative ^{6}Li NMR approach. The ^{6}Li peak intensities presented by NMR data represent the total lithium content in the materials. Data points were selected along the charge/discharge profiles in order to follow structural changes that occur at key potentials based on the previously proposed model of hysteresis and voltage fade (Figure 1a and refs 8 and 10).

Two main groups of resonances are generally observed in the ^{6}Li NMR spectra of pristine, layered lithium- and manganese-rich transition-metal oxide structures, one between 500 and 800 ppm and another between 1300 and 1500 ppm, assigned to lithium in the lithium layers (Li_{Li}) and lithium in the TM layers (Li_{TM}), respectively. These well-established lithium resonances arise from the Fermi-contact interactions of first and second coordination shell, paramagnetic nickel (Ni^{2+}) and manganese (Mn^{4+}) ions[29] (Tables S2 and S3). A detailed discussion on lithium environments in pristine and activated materials (end of first cycle) is also given in Supporting Information, p S5. At 2.0 V (point 1, Figure 1a), before the start of the second cycle, a pronounced intensity loss for the TM layer lithium environments is already observed relative to the pristine material

DOI: 10.1021/ja511299y
J. Am. Chem. Soc. 2015, 137, 2328−2335

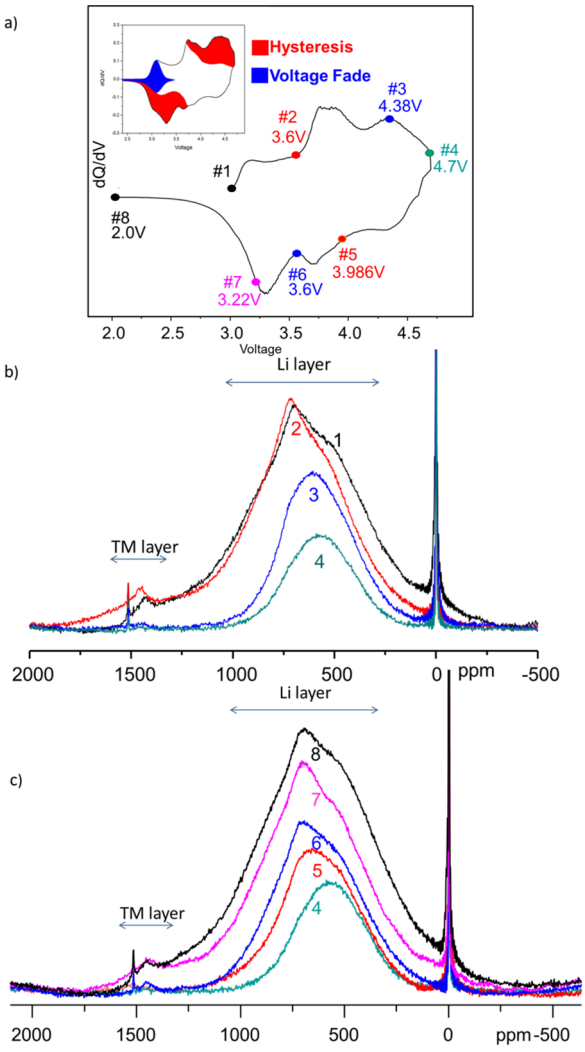

Figure 1. (a) Second cycle dQ/dV plot with labels corresponding to voltages at which NMR spectra were acquired. The corresponding SOCs are given in Table S1. Inset shows the schematic representation of electrochemical hysteresis and voltage fade with respect to dQ/dV during second cycle charge/discharge. Point 1 was stopped at 2.0 V after first cycle and allowed to relax. (b and c) ^{6}Li MAS NMR at various SOCs along the second cycle charge and discharge, respectively.

(Figure S2), indicating that not all Li_{TM} are reinserted during the first discharge, accompanied by considerable ^{6}Li peak broadening due to a profound loss of order in the material (Figure 1c). During the early stages of the second cycle charge (points 1 and 2, Figure 1a,b), removal of Li_{Li} from nickel-rich environments (~540 and ~890 ppm, assignment details in Supporting Information, p S5), concomitant with a slight shift and removal of Li in the Li_{Li} region at ~720 ppm, is observed due to rearrangement of TMs. At 4.38 V (point 3), simultaneous removal of Li_{Li} and Li_{TM} is observed with a considerable loss of intensity for Li_2MnO_3-like (~720 ppm) and nickel-rich environments (~890 ppm). At the top of charge, 4.7 V, ~75% of the initial Li-ions are removed from the structure with the remaining ~25% residing in the lithium layers (Li_{Li}). These remaining lithium can be assigned to Li-ions that have migrated into lithium-layer tetrahedral sites adjacent to vacated octahedral sites of the TM layers, creating low energy, stable lithium-dumbbell configurations (Li_{Tet}-□-TM_{Tet}/Li_{Tet}).[14,23,31]

Interestingly, between points 1 and 2 (≤3.6 V), the electrochemical region that grows in capacity with cycling (i.e., voltage fade phenomenon),[10] an unusual ^{6}Li peak evolution in the ~1600 ppm (TM-layer) region is captured for the first time, indicating a new ordering for Li_{TM}. It has to be noted that although there is lithium removal from the system at points 1 to 2, there is a clear increase in ^{6}Li-peak intensity associated with the TM layer region. The same ^{6}Li peak formation is once again observed during the subsequent lithium insertion at 3.986 V (point 5) and between 3.2 and 2.0 V (points 7 and 8) where electrochemical hysteresis is observed (Figure 1a,c). Once again, lithium peaks are formed at point 7 (~1600 ppm), and the intensity is lost when 2.0 V is reached (point 8). This observation suggests that between points 1 and 2, lithium local environments go through a re-entrant process which was already initiated during the first discharge between 3.2 and 2.0 V. The re-entrant behavior repeats itself, with repetitive cycles, within the hysteresis and voltage fade loops (Figure 4). The presence of these lithium environments indicates significant changes in TM coordination to lithium, i.e., formation of TM defects via migration. The basis of the assignments and the nature of the defect TM sites will be discussed in detail in the next section. A similar resonance might have been observed in a previous study[14] but not assigned due to poor signal-to-noise. The ability to reliably track the intensity of this feature highlights an important aspect, namely, the intentional use of ^{6}Li enriched cell components in this study.

^{6}Li MAS NMR spectra during lithium insertion from 4.7 V down to 2.0 V, including points at 3.986, 3.6, and 3.22 V (Figure 1a), on the second cycle discharge are shown in Figure 1c. A comparison of the NMR spectra given in Figure 1b,c simply reveals that lithium extraction and insertion do not follow the same order. From the end of the second charge (4.7 V, point 4), relithiation starts with Li_2MnO_3-like, ordered lithium sites (sharp peak at ~710 ppm) and distorted lithium layer sites (Li_{Li}) (broad, Gaussian peak ~668 ppm, see Figure S3 for representative deconvolution). No significant lithium occupancy is seen for the nickel-rich environments (540 ppm and lower) until 3.6 V (point 6), although these sites were the first to be removed during the previous charge. This is consistent with previous reports on slow occupation of lithium sites next to Ni^{2+}, within lithium layers.[25] At lower voltages, between 3.22 and 2 V (points 7 and 8), the resonances due to nickel rich environments at ~870 and ~540 ppm re-emerge along with an intensity increase for distorted Li_{Li} (~668 ppm Gaussian peak). During discharge, only ~7% of the initial Li_{TM} are reinserted back into TM layers where a drastic increase in occupation of these sites is observed between ~3.6 and ~3.2 V (points 6 and 7), as seen by peak formation between 1250 and 1500 ppm (Figure 1c).

The structure−activity relationship can be revealed in further detail by comparing ^{6}Li NMR data on points selected with various SOCs, but with equivalent lithium contents, to observe the differences in lithium site occupancies (Figure 2). For instance, at point 3 (Figure 2a), for a cell charged to 4.38 V, a mixture of lithium in dumbbells and lithium in octahedral sites in lithium layers is observed. However, a different local ordering is observed for a cell having the same Li content, but which was first charged all the way to 4.7 V and then discharged to 3.986 V (point 5). The last lithiums that are removed from Li_{Li} on

DOI: 10.1021/ja511299y
J. Am. Chem. Soc. 2015, 137, 2328−2335

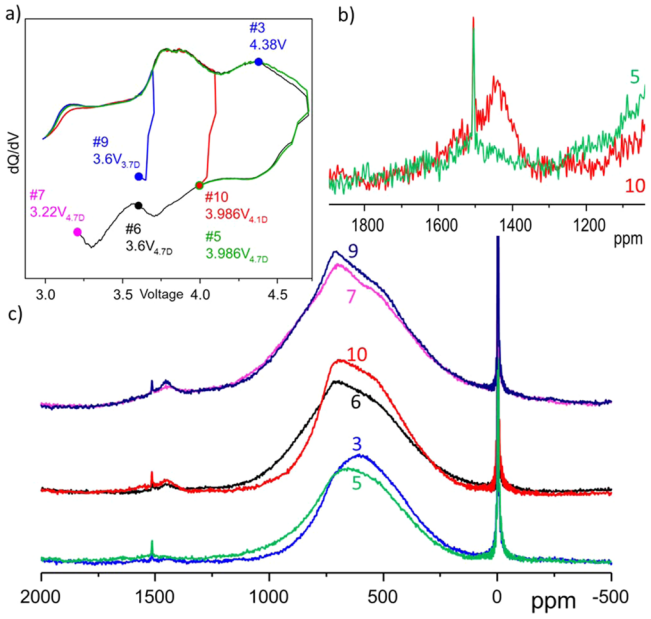

Figure 2. (a) dQ/dV plots for several samples charged/discharged to equivalent lithium contents and the corresponding voltages as labeled. Sample numbers correspond to the NMR spectra in (b and c). (b) Magnified view of lithium environments in the TM region for points 5 and 10. (c) ^{6}Li MAS NMR of $0.5Li_2MnO_3{\cdot}0.5LiMn_{0.5}Ni_{0.5}O_2$ comparing samples charged/discharged to equivalent lithium contents.

charge are not the first sites to be lithiated on discharge, i.e., hysteresis. This effect of cycling above 4.1 V and accessing the hysteresis component is further highlighted in Figure 2b (points 5 and 10). The spectra reveal that Li_{TM} is not removed until charging above 4.1 V and is not reinserted into the structure until at least after 3.986 V on discharge. In another instance, a significant change in lithium ordering is observed in sample 6, which has undergone a charge to 4.7 V followed by discharge to 3.6 V, relative to sample 10 having the same Li content as 6, which was only charged to 4.1 V. These correlate well with the electrochemical hysteresis component in the high voltage region (above 4.1 V, Figure 1a inset). On the other hand, the hysteresis voltage difference these materials exhibit can be shown structurally by comparing points 9 and 7. A cell that is cycled to high voltage which accesses the hysteresis component (point 7) must be discharged to a significantly lower voltage (~1 V) before the Li ordering is similar to a cell without the high voltage charging (point 9).

These data related to local lithium structure and site occupancy correlate well with the electrochemical hysteresis observed and with an earlier report showing hysteresis in TM oxidation states as a function of SOC in LMR-NMCs.[8,10] This remarkable 1 V hysteresis is correlated to the defect sites discussed in the next section.

Capturing Partially Reversible Electrochemically Induced Transition-Metal Migration. Although transition-metal migration has been a long-standing phenomenon[13−15,22] thought to accompany the complex structural transformation(s) observed for lithium rich transition-metal oxides, no direct and conclusive spectroscopic evidence with a lithium local probe for this activity has been shown. Here we present a ^{6}Li MAS NMR approach to capture TM migration via its effect on the local structure around Li-ions and its direct effect on electrochemical activity for the first time. For spectra observed at points 2 and 7, in Figure 1b,c, a broad high frequency ^{6}Li peak is observed at 1600 ppm. This peak is first observed at low voltages, post-activation, and on charge and appears once again on discharge.

In order to have a total hyperfine shift for a Li_{TM} resonance at ~1600 ppm, additional TMs must be coordinated to $LiMn_6$ units via the presence of a tetrahedral or octahedral TM in the layers immediately above or below. This can be concluded based on previous ^{6}Li NMR chemical shift values reported on similar cathode materials and our heuristic shift calculations (see Tables S2 and S3) and is shown schematically for tetrahedral manganese in Figure 3 for a partially delithiated

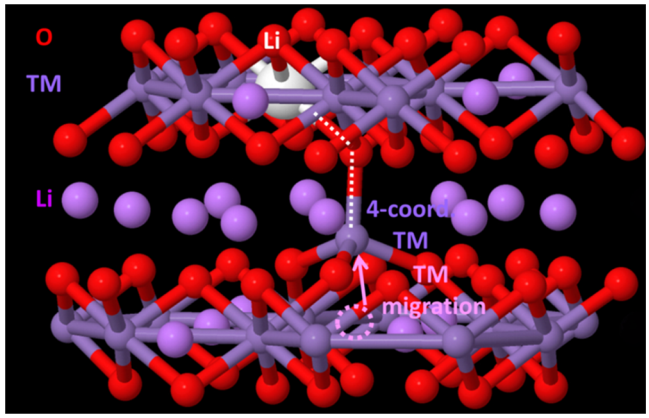

Figure 3. Structural representation of tetrahedral TM (dark purple) coordinated to lithium (white) in the TM layer of a partially delithiated layered, oxygen vacancy bearing $LiTMO_2$ lattice.

oxygen vacancy bearing lattice. This assignment represents the first direct ^{6}Li NMR observation of Li-TM coordination changes and TM migration via the shift effect on Li_{TM} resonances at specific states of charge. This new ^{6}Li resonance is now denoted as $LiTM_6$-$TM_{tet/oct}$. The relative intensity loss of the lithium sites associated with $LiTM_6$-$TM_{tet/oct}$ defects (~1600 ppm) from charge to discharge (Figure 1, comparing points 2 and point 7, respectively) indicates limited reversibility of the spectroscopically detected TM migration. This correlates directly with the proposed model of hysteresis and voltage fade where partially reversible TM migration is indicated as a key mechanism.[10] Further information regarding the presence of a tetrahedral Mn (compared to reference[39]) can be found in the DFT calculation section in Supporting Information, p S11.

In order to study the evolution of resonances arising from $LiTM_6$-$TM_{tet/oct}$ defects, detailed deconvolutions of the NMR data at specific SOCs have been analyzed. Figure 5a−c shows the deconvoluted spectra for cells charged to 3.6 V on cycles 2, 11, and 20, respectively. The 1600 ppm region involves two distinct, small peaks at ~1550 and 1688 ppm. The former (1550 ppm) likely indicates the presence of tetrahedral Mn (Mn_{tet} added shift of +80 ppm[29,30,32,33]) but could also be attributed to the presence of octahedral Ni^{3+} in the lithium layers (added shift of +110 ppm[38]). Li−Ni exchange and Ni occupancy in lithium layers have been shown, in pristine materials, in earlier studies.[23,24,26,27] However, Li-ions are assumed to be removed from the vicinity (first and second coordination shell) of oxidized Ni (+3 and +4), corresponding to electrochemical activity.[29] Furthermore, the distinct loss of ordering observed for the Li_2MnO_3-like coordinations (724 and 765 ppm) post-activation indicates Mn activity/migration. In addition to this, spectra collected along the first cycle at similar

DOI: 10.1021/ja511299y
J. Am. Chem. Soc. 2015, 137, 2328−2335

data points presented herein, for a system where nickel is substituted with cobalt (see Figure S4), have produced very similar shifts suggesting that the TM activity observed arises predominantly from Mn_{tet}. Therefore, 1550 ppm resonance has been assigned to $LiMn_6$-Mn_{tet}. Interestingly, the detected migration does not occur within an electrochemical window where Mn^{3+} forms, a requirement shown for Mn migration in layered oxides.[39] This migration possibility has previously been proposed by us for lithium and manganese rich metal oxides.[40] The assignment of the component responsible for the 1688 ppm is more complex—likely involves either Mn_{oct} or Ni^{2+} in Li layer, just above or below the $LiMn_6$ unit. However, the absence of 1688 ppm component in Li_2MnO_3:$LiCoO_2$ sample suggests the presence of $LiMn_6$-Ni_{oct}. Further details of the basis of these assignments are provided in the Supporting Information, p S5–S6.

Figure 4 compares samples cycled to the same voltage (3.6 V) but with different charge voltages, resulting in different

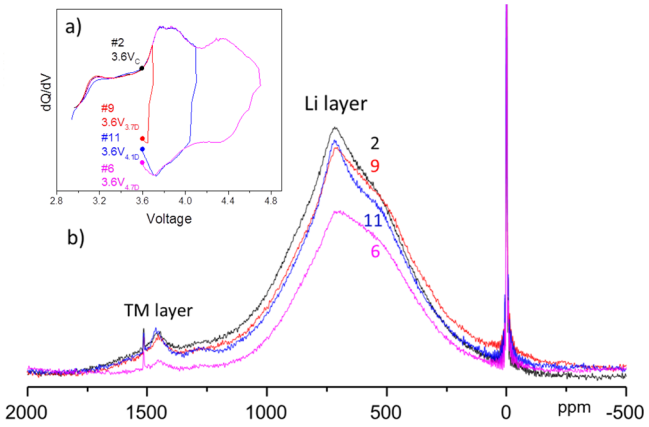

Figure 4. (a) dQ/dV plot with labels corresponding to voltages at which NMR spectra were acquired and (b) ^{6}Li MAS NMR of cells at the same voltage; with different charge voltage switching potential and resultant states of charge.

states of charge. The data points were selected to capture additional Mn_{tet} coordination and the effect of hysteresis on local structure with respect to upper cutoff voltage for the charge. As shown with the ^{6}Li NMR data of point 11, charge voltage of 4.1 V, Li_2MnO_3-like ordering still exists as both Li_{Li} and Li_{TM} orderings are present. A small peak around 1300 ppm is observed for the first time for this sample which might be due to Li ordering in TM layers with nickel neighboring, as the lower Fermi contact interaction can be the result of presence of diamagnetic Ni^{4+}. Charging beyond 4.1 V extracts Li from both Li and TM layers causing disorder and loss of Li_2MnO_3-like ordering (point 6). More importantly, comparison of point 6 vs points 11 and 7 illustrates that for a sample charged beyond 4.4 V, i.e., the high voltage plateau, the local order can only be restored to the precharge state by discharging beyond 3.4 V, i.e., low voltage plateau. This 1 V hysteresis can directly be observed structurally and correlated directly to the remarkable re-entrant $LiMn_6Mn_{tet}$ coordinations for the spectra of points 2, 6, 9, and 11 and point 7 (Figures 4 and 1c).

Besides the significance of the migrated TM assignments described above, one important point to note is the dramatically low concentrations of lithium coordinations associated with these migrated TMs (see green and blue areas in Figure 5a,b). The approximate quantification of the integrated areas for 1550 and 1688 ppm regions indicates that only ~1.9% and 1.2% of the overall lithium content are associated with $LiTM_6$-$TM_{tet/oct}$ coordinations, respectively. These results are again remarkable, such that, the effect of transition-metal migration/coordination change and defect formation on lithium local environment is small with respect to the 1 V electrochemical hysteresis observed. It is only through the use of very high signal-to-noise, ^{6}Li NMR data, and full quantification that detection of these defects is made possible.

The effect of increasing cycle number on the intensity of $LiMn_6$-Mn_{tet} and $LiMn_6$-Ni_{oct} resonances (1550 and 1688 ppm) has also been studied. Figure 5d shows cells that have been charged to 3.6 V on cycles 2, 11, and 20. As shown with the highlighted peak area comparisons and approximate % integration values (Figure 5a–c), the intensities and relative frequencies of these lithium environments decrease subtly with increasing cycle number (from a combined approximate 3.2% on cycle 2 to ~2.7% by cycle 11 and ~1.9% by cycle 20). This loss of intensity can also be visually followed in 1600 ppm region in the normalized Figure 5d. A minor contribution to the loss of intensity also comes from capacity loss (about 11.6% of the total intensity loss after 11 cycles). This correlates well with stabilization of TM ordering, i.e., a decrease in TM migration and a slowing down of the electrochemical voltage fade phenomenon. It is also significant to note that with a few percent TM migration and defect site formation, a 1 V hysteresis is created involving 10% lithium removed above 4 V and inserted back in the structure below 3.5 V. This is a clear and important example of defect sites governing structural and electrochemical activities.

Evolution of Li/TM Ordering, Cycle Number, and Voltage Fade. The TM migration phenomenon highlighted in the spectroscopic results (Figure 5) has profound effects on the lithium order of the fully discharged electrodes. As the electrochemical signatures of voltage fade appear in the dQ/dv plots for the cycled electrodes, ^{6}Li NMR data shows a clear center of mass shift of about 100 ppm to lower frequencies for the Li_{Li} at points collected at the bottom of discharge after 1,2 and 11 cyles (Figures 6a,b and S4). The overall intensity for all spectra in Figure 6a are normalized in Figure 6b mitigating the effects of any capacity loss with cycling and to better visualize the shift in frequency. Resonances traditionally assigned to Li_{Li} mainly contribute to the center of mass shift (Gaussian peak shifts from 668 to 556 ppm from cycle 2 to cycle 20 (Figure S4). As discussed in our previous studies, the changes observed in local lithium environments that are correlated with voltage fade slow down significantly after ~40 cycles.[41−43] By taking into account the evidence for partially reversible TM migration for each cycle, post-activation, it is believed that there must be some contribution of lithium coordinated to the migrated TMs to the shift in the Gaussian resonance (predominantly manganese rich coordinations, Supporting Information, p S13) and tentatively to undercoordination (such as nondumbbell Li_{tet}).[41−43] At this point, the resonance and corresponding local structures can no longer be assigned only to the formal Li_{Li} or Li_{TM}. Furthermore, the concentration of these lithium environments is sufficient (~30%) to create a gradual loss of average voltage due to changes *only* in local structures and giving rise to lower lithium site energies.[41−43] Other contributing mechanisms to the voltage loss can be coherency strain induced on the lithium sites via distortions, which are

DOI: 10.1021/ja511299y
J. Am. Chem. Soc. 2015, 137, 2328−2335

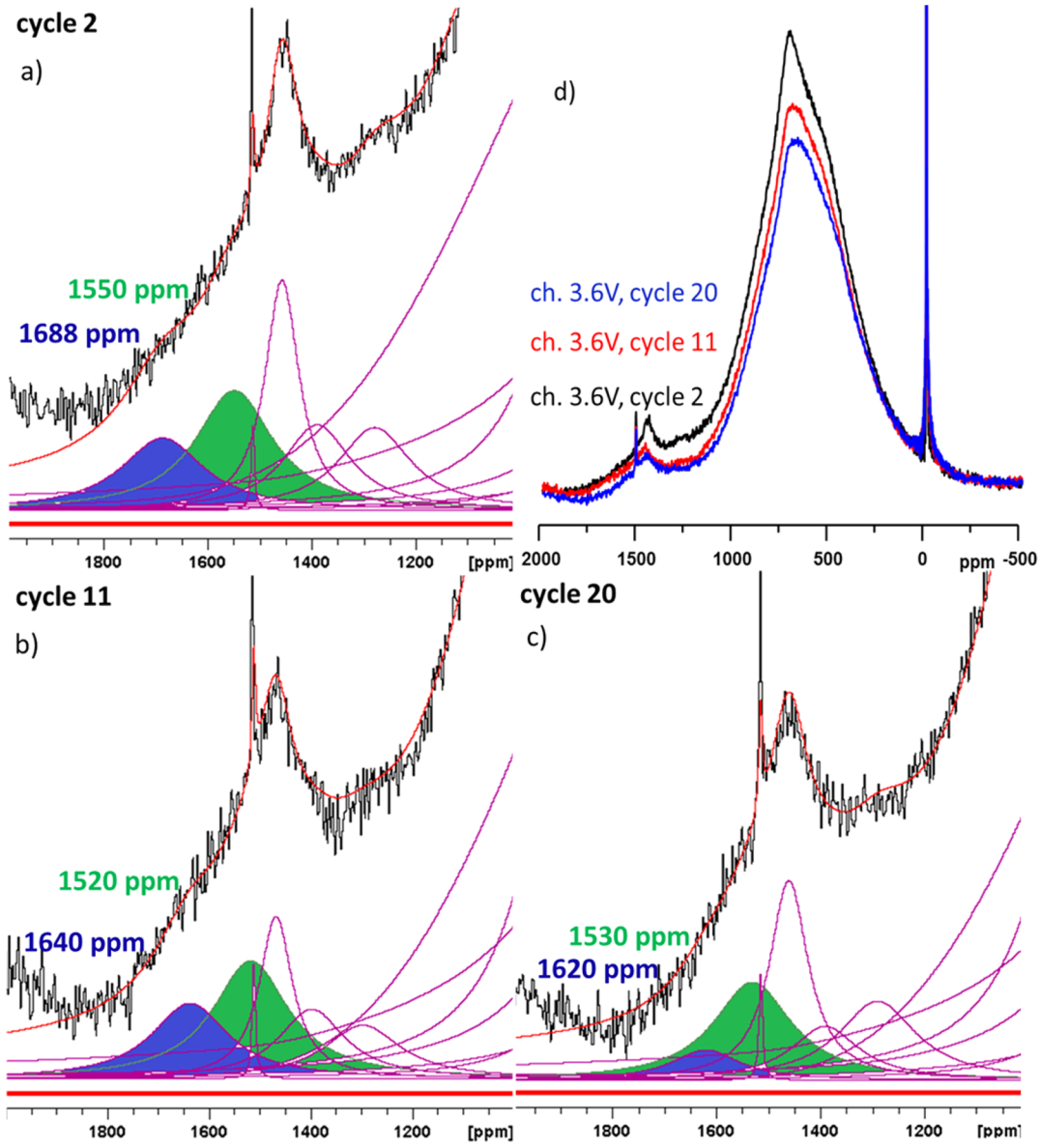

Figure 5. Effect of increasing cycle number on ^{6}Li MAS NMR of $0.5Li_2MnO_3{\cdot}0.5LiMn_{0.5}Ni_{0.5}O_2$ electrodes charged to 3.6 V. (a–c) ^{6}Li MAS NMR deconvolutions for Li_{TM} region for cycles 2, 11, and 20, respectively. Blue and green peaks show the lithium peaks coordinated to octahedral nickel and tetrahedral manganese, respectively. Lithium contents for the specific sites were calculated with the integrated area of the corresponding lithium peak within the mass normalized spectra. The approximate values are 1.9%, 1.7%, 1.5% for manganese site and 1.2%, 1.1%, and 0.5% for nickel site after 2, 11, and 20 cycles, respectively. (d) Full spectrum ^{6}Li MAS NMR comparison of 2, 11, and 20 cycles.

clearly captured by NMR as observed in significant broadening of peaks with cycling.

Overall, the analysis and spectral interpretations performed in this study have been found to support the proposed mechanisms of hysteresis and voltage fade hypothesized earlier (Figure 6c and ref 10) by directly monitoring the local structural changes that occur in Li-rich electrodes. Finally, it has to be noted that ^{6}Li MAS NMR spectra only relate to the local structure around Li-ions that still exists in the material being studied and is an averaging probe that does not readily distinguish between core of the particles and the outer surface. Given the volume averaging nature of the probed signal, no arguments on the preferential location of the defects can be easily provided, unlike those evidently seen in transmission electron microscopy studies.[16,17] Possible oxygen charge compensation phenomenon[16] at higher states of charge would correspond to minimum Li coordination due to delithiation in the immediate vicinity; therefore, these environments will be largely unrepresented in ^{6}Li NMR spectra. The possible effects on the NMR spectra of charge compensation by oxygen at high states of delithiation (e.g., 4.7 V) are expected to have minimum to zero contribution in the highly lithiated states (e.g., $< \sim 3.6$ V) where the critical observations herein have been made.

■ CONCLUSIONS

This study has helped to identify structural causes of reversible hysteresis and voltage fade phenomena observed for Li-rich composite materials. There are two main structural processes identified from the experimental results obtained: (1) Lithium removal and reinsertion from and into the activated composite structure are found to be path dependent in terms of Li-sites,

DOI: 10.1021/ja511299y
J. Am. Chem. Soc. 2015, 137, 2328–2335

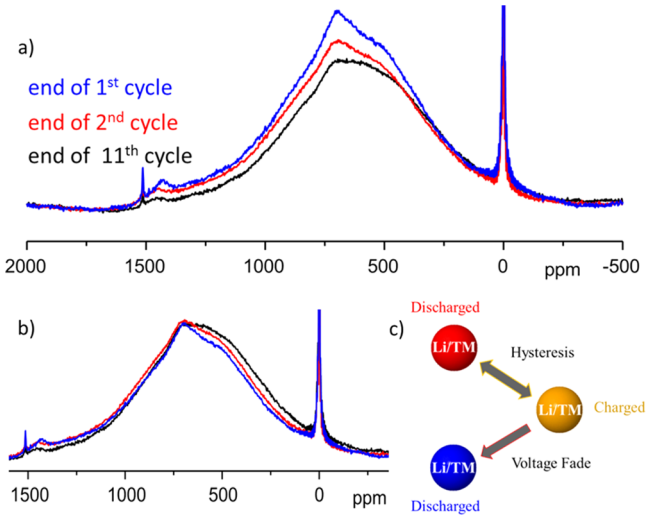

Figure 6. (a) Mass-normalized and (b) non-normalized ^{6}Li MAS NMR of cells at zero state of charge for increasing cycle number. (c) Schematic correlation of hysteresis and voltage fade.[10]

i.e., structural hysteresis. The structural hysteresis is found to be reversible and correlates directly with electrochemical hysteresis. Furthermore, it is dependent on a remarkably low concentration of defect sites formed upon activation within the electrode structure. (2) Defect ^{6}Li sites are observed due to a hyperfine shift of tetrahedral TMs coordinated to $LiMn_6$ units above or below of the lithium layer as well as TMs in octahedral lithium sites. This process indicates electrochemically induced TM migration and is found to be only partially reversible. The resulting partial TM re-ordering in only the *local* structure correlates directly with the 1 V electrochemical hysteresis and voltage fade due to, presumably, lowered Li-site energies without corresponding to any new distinct long-range order (spinel).

These two processes have been found to progress simultaneously, post-activation, upon cycling and bolster the spectroscopic evidence in support of the structural hysteresis and voltage fade model previously proposed for Li- and Mn-rich composite electrodes. The TM defect sites and re-entrant lithium environments are a brand new find, reported for the first time spectroscopically, and even in very small percentages define an entire electrochemistry.

■ ASSOCIATED CONTENT

Supporting Information

Description electrochemical methodology, details on NMR characterization methods and spectral assignment strategies and supporting discussions, theoretical calculation methodology and supporting discussions. This material is available free of charge via the Internet at http://pubs.acs.org.

■ AUTHOR INFORMATION

Corresponding Authors

*mali@aps.anl.gov
*bkey@anl.gov

Author Contributions

‖These authors contributed equally.

Notes

The authors declare no competing financial interest.

■ ACKNOWLEDGMENTS

Support from the Vehicle Technologies Program, Hybrid and Electric Systems, in particular, David Howell, Tien Duong, and Peter Faguy, at the U.S. Department of Energy, Office of Energy Efficiency and Renewable Energy are gratefully acknowledged. The submitted manuscript has been created by UChicago Argonne, LLC, Operator of Argonne National Laboratory ("Argonne"). Argonne, a U.S. Department of Energy Office of Science laboratory, is operated under contract no. DE-AC02-06CH11357.

■ REFERENCES

(1) Armand, M.; Tarascon, J. M. *Nature (London, U. K.)* **2008**, *451*, 652.
(2) Tarascon, J. M.; Armand, M. *Nature* **2001**, *414*, 359.
(3) Gallagher, K. G.; Goebel, S.; Greszler, T.; Mathias, M.; Oelerich, W.; Eroglu, D.; Srinivasan, V. *Energy Environ. Sci.* **2014**, *7*, 1555.
(4) Zhonghua, L.; Beaulieu, L. Y.; Donaberger, R. A.; Thomas, C. L.; Dahn, J. R. *J. Electrochem. Soc.* **2002**, *149*, A778.
(5) Thackeray, M. M.; Kang, S.-H.; Johnson, C. S.; Vaughey, J. T.; Benedek, R.; Hackney, S. A. *J. Mater. Chem.* **2007**, *17*, 3112.
(6) Croy, J. R.; Gallagher, K. G.; Balasubramanian, M.; Long, B. R.; Thackeray, M. M. *J. Electrochem. Soc.* **2014**, *161*, A318.
(7) Long, B. R.; Croy, J. R.; Dogan, F.; Suchomel, M. R.; Key, B.; Wen, J.; Miller, D. J.; Thackeray, M. M.; Balasubramanian, M. *Chem. Mater.* **2014**, *26*, 3565.
(8) Croy, J. R.; Gallagher, K. G.; Balasubramanian, M.; Chen, Z.; Ren, Y.; Kim, D.; Kang, S.-H.; Dees, D. W.; Thackeray, M. M. *J. Phys. Chem. C* **2013**, *117*, 6525.
(9) Bettge, M.; Li, Y.; Gallagher, K.; Zhu, Y.; Wu, Q.; Lu, W.; Bloom, I.; Abraham, D. P. *J. Electrochem. Soc.* **2013**, *160*, A2046.
(10) Gallagher, K. G.; Croy, J. R.; Balasubramanian, M.; Bettge, M.; Abraham, D. P.; Burrell, A. K.; Thackeray, M. M. *Electrochem. Commun.* **2013**, *33*, 96.
(11) Mohanty, D.; Sefat, A. S.; Li, J.; Meisner, R. A.; Rondinone, A. J.; Payzant, E. A.; Abraham, D. P.; Wood, D. L., III; Daniel, C. *Phys. Chem. Chem. Phys.* **2013**, *15*, 19496.
(12) Ohzuku, T.; Nagayama, M.; Tsuji, K.; Ariyoshi, K. *J. Mater. Chem.* **2011**, *21*, 10179.
(13) Armstrong, A. R.; Holzapfel, M.; Novak, P.; Johnson, C. S.; Kang, S. H.; Thackeray, M. M.; Bruce, P. G. *J. Am. Chem. Soc.* **2006**, *128*, 8694.
(14) Jiang, M.; Key, B.; Meng, Y. S.; Grey, C. P. *Chem. Mater.* **2009**, *21*, 2733.
(15) Koga, H.; Croguennec, L.; Ménétrier, M.; Mannessiez, P.; Weill, F.; Delmas, C.; Belin, S. *J. Phys.Chem.C* **2014**, *118*, 5700.
(16) Genevois, C.; Koga, H.; Croguennec, L.; Ménétrier, M.; Delmas, C.; Weill, F. *J. Phys. Chem. C* **2014**, *119*, 75.
(17) Boulineau, A.; Simonin, L.; Colin, J.-F.; Bourbon, C.; Patoux, S. *Nano Lett.* **2013**, *13*, 3857.
(18) Kim, S.; Ma, X.; Ong, S. P.; Ceder, G. *Phys. Chem. Chem. Phys.* **2012**, *14*, 15571.
(19) Ma, X.; Hautier, G.; Jain, A.; Doe, R.; Ceder, G. *J. Electrochem. Soc.* **2013**, *160*, A279.
(20) Armstrong, A. R.; Dupre, N.; Paterson, A. J.; Grey, C. P.; Bruce, P. G. *Chem. Mater.* **2004**, *16*, 3106.
(21) de Picciotto, L. A.; Thackeray, M. M.; David, W. I. F.; Bruce, P. G.; Goodenough, J. B. *Mater. Res. Bull.* **1984**, *19*, 1497.
(22) Balasubramanian, M.; McBreen, J.; Davidson, I. J.; Whitfield, P. S.; Kargina, I. *J. Electrochem. Soc.* **2002**, *149*, A176.
(23) Breger, J.; Meng, Y. S.; Hinuma, Y.; Kumar, S.; Kang, K.; Shao-Horn, Y.; Ceder, G.; Grey, C. P. *Chem. Mater.* **2006**, *18*, 4768.
(24) Kang, K. S.; Meng, Y. S.; Breger, J.; Grey, C. P.; Ceder, G. *Science* **2006**, *311*, 977.
(25) Van der Ven, A.; Ceder, G. *Electrochem. Commun.* **2004**, *6*, 1045.
(26) Breger, J.; Dupre, N.; Chupas, P. J.; Lee, P. L.; Proffen, T.; Parise, J. B.; Grey, C. P. *J. Am. Chem. Soc.* **2005**, *127*, 7529.

DOI: 10.1021/ja511299y
J. Am. Chem. Soc. 2015, 137, 2328−2335

(27) Bréger, J.; Jiang, M.; Dupré, N.; Meng, Y. S.; Shao-Horn, Y.; Ceder, G.; Grey, C. P. *J. Solid State Chem.* **2005**, *178*, 2575.
(28) Carlier, D.; Menetrier, M.; Grey, C. P.; Delmas, C.; Ceder, G. *Phys. Rev. B* **2003**, *67*, 174103.
(29) Grey, C. P.; Dupre, N. *Chem. Rev. (Washington, DC, U.S.)* **2004**, *104*, 4493.
(30) Grey, C. P.; Lee, Y. J. *Solid State Sci.* **2003**, *5*, 883.
(31) Grey, C. P.; Yoon, W. S.; Reed, J.; Ceder, G. *Electrochem. Solid-State Lett.* **2004**, *7*, A290.
(32) Lee, Y. J.; Grey, C. P. *J. Phys. Chem. B* **2002**, *106*, 3576.
(33) Lee, Y. J.; Wang, F.; Grey, C. P. *J. Am. Chem. Soc.* **1998**, *120*, 12601.
(34) Pan, C. J.; Lee, Y. J.; Ammundsen, B.; Grey, C. P. *Chem. Mater.* **2002**, *14*, 2289.
(35) Yoon, W. S.; Iannopollo, S.; Grey, C. P.; Carlier, D.; Gorman, J.; Reed, J.; Ceder, G. *Electrochem. Solid-State Lett.* **2004**, *7*, A167.
(36) Yoon, W.-S.; Kim, N.; Yang, X.-Q.; McBreen, J.; Grey, C. P. *J. Power Sources* **2003**, *119−121*, 649.
(37) Younkee, P.; Grey, C. P.; Johnson, C. S.; Jeom-Soo, K.; Thackeray, M. M. *Chem. Mater.* **2002**, *14*, 5109.
(38) Zeng, D.; Cabana, J.; Breger, J.; Yoon, W.-S.; Grey, C. P. *Chem. Mater.* **2007**, *19*, 6277.
(39) Reed, J.; Ceder, G.; Van Der Ven, A. *Electrochem. Solid-State Lett.* **2001**, *4*, A78.
(40) Balasubramanian, M., Croy, J. R., Gallagher, K. G. X-ray and Neutron Methods to Understand Voltage Fade. Proceedings of the U.S. Drive Meeting, Argonne National Laboratory, Argonne, IL, January, 2013; Argonne National Laboratory: Argonne, IL, 2013.
(41) Dogan, F.; Croy, J. R.; Balasubramanian, M.; Slater, M. D.; Iddir, H.; Johnson, C. S.; Vaughey, J. T.; Key, B. *J. Electrochem. Soc.* **2015**, *162*, A235.
(42) Key, B., Dogan, F., Croy, J. R., Slater, M. D., Balasubramanian, M., Yang, R., Johnson, C. S., Vaughey, J. T. Solid State NMR Studies of Li-Rich NMC Cathodes: Investigating Structure Change and Its Effect On Voltage Fade Phenomenon, Abstract 809. Proceedings of the 224th Electrochemical Society (ECS) Meeting,San Francisco, CA, October 27 − November 1, 2013; ECS: Pennington, NJ, 2013
(43) Key B., Dogan F., Long B. R., Croy J. R., Balasubramanian M., Slater M. D., Iddir H., Benedek R., Bettge M., Johnson C. S., Vaughey J. T., Solid State NMR Studies of Li-Rich NMC Cathodes: Investigating Structure Change and Its Effect on Voltage Fade Phenomenon. Proceedings of the DOE Hydrogen Program and Vehicle Technologies Program Annual Merit Review, Washington, DC, June 16−20, 2014, U. S. Department of Energy: Washington, DC, 2014; p ES187.

DOI: 10.1021/ja511299y
J. Am. Chem. Soc. 2015, 137, 2328−2335